Lab on a Chip

Wireless, passive strain sensor in a doughnut-shaped contact lens for continuous non-invasive self-monitoring of intraocular pressure

Journal:	*Lab on a Chip*
Manuscript ID	LC-ART-07-2019-000735
Article Type:	Paper
Date Submitted by the Author:	28-Jul-2019
Complete List of Authors:	Mazaheri Kouhani, Mohammad Hossein; Michigan State University, Electrical and computer engineering Wu, Jiajia; Michigan State University, Electrical and computer engineering Tavakoli, Arman; Michigan State University, Mathematics Weber, Arthur; Michigan State University, Physiology Li, Wen; Michigan State University, Electrical and computer engineering

Article type: Full paper

Lab on a Chip

Devices and applications at the micro- and nanoscale

Website www.rsc.org/loc

Impact factor* 5.995

Journal expectations To be suitable for publication in *Lab on a Chip*, articles must report significant and original work related to miniaturisation, at the micro- and nano-scale, of interest to a multidisciplinary readership. The journal seeks to publish work at the interface between physical technological advancements and high impact applications that are of direct interest to a broad audience.

Visit the journal website for additional details of the journal scope and expectations.

Article type: Full paper Original scientific work that has not been published previously. Full papers must represent a significant development in the particular field, and are judged according to originality, quality of scientific content and contribution to existing knowledge. Full papers do not have a page limit and should be appropriate in length for scientific content. Further information on article types can be found on our website.

Please consider these high standards when making your recommendation to accept or reject. It is essential that all articles submitted to *Lab on a Chip* meet the significant novelty criteria; lack of novelty is sufficient reason for rejection**.**

Reviewer responsibilities Visit the Reviewer responsibilities website for additional details of the reviewing policy and procedure for Royal Society of Chemistry journals.

When preparing your report, please:

- Use the journal scope and expectations to assess the manuscript's suitability for publication in *Lab on a Chip.*
- Comment on the originality, importance, impact and reliability of the science. English language and grammatical errors do not need to be discussed in detail, except where it impedes scientific understanding.
- State clearly whether you think the paper should be accepted or rejected, giving detailed comments that will both help the Editor to make a decision on the paper and the authors to improve it.
- Inform the Editor if there is a conflict of interest, a significant part of the work you cannot review with confidence or if parts of the work have previously been published.
- Provide your report rapidly and within the specified deadline, or inform the Editor immediately if you cannot do so

You can submit you report at https://mc.manuscriptcentral.com/lc

Thank you for evaluating this manuscript, your advice as a reviewer for *Lab on a Chip* is greatly appreciated. To acknowledge this, the Royal Society of Chemistry offers a **25% discount** on our books: http://www.rsc.org/Shop/books/discounts.asp.

Yours sincerely,

Dr Simon Neil
Executive Editor
Royal Society of Chemistry

Professor Abraham Lee
Editor-in-Chief
University of California, Irvine, USA

**2017 Journal Citation Reports®, (Clarivate Analytics, 2018)*

ARTICLE

Wireless, passive strain sensor in a doughnut-shaped contact lens for continuous non-invasive self-monitoring of intraocular pressure

M. Hossein M. Kouhani[1], Jiajia Wu[1], Arman Tavakoli[2], Arthur J. Weber[3], Wen Li[1]

Received 00th January 20xx,
Accepted 00th January 20xx

DOI: 10.1039/x0xx00000x

After Cataract, glaucoma is the second leading cause of blindness worldwide and real-time monitoring of intraocular pressure (IOP) is of great demand. We present a wireless, passive sensor sitting inside a customized, planar and circular doughnut-shaped contact-lens capable of continuous monitoring of change in the curvature of cornea caused by IOP fluctuations. The sensor consists of a constant capacitor and a variable inductor in form of a stretchable, closed-loop, serpentine wire that serves as both the sensor and the antenna. Results show a pressure responsivity of 523 kHz per 1% axial strain on a pressurized Polydimethylsiloxane membrane and 44 kHz per 1 mmHg of change in IOP of a canine eye. The sensor is tested for stability and shows unvaried characteristics after repeated cycles and parasitic movements. Predictable influences of temperature and humidity on sensor response are also verified experimentally, which can be canceled out using real-time calibration with temperature and humidity sensors to integrate with a reader device. The design reported here has numerous advantages, such as design simplicity, component reliability, high responsivity, and low cost, thereby opening up potential opportunities for the translation of this non-invasive, continuous IOP monitoring technique into clinical applications.

INTRODUCTION

Vision is the most critical human sensory domain in creating the perception of the world. According to a national survey of 2,044 U.S. residents in 2016, most Americans across all ethnic and racial groups describe losing eyesight as having the greatest impact on their quality of life when compared against other outcomes such as loss of limb, memory, hearing or speech [1]. Among all eye diseases, glaucoma is the second leading cause of blindness worldwide and is expected to cause 11.2 million cases of irreversible blindness globally by 2020 [2]. It is a multifactorial and complex eye disease that is strongly associated with elevated intraocular pressure (IOP). Normal eye pressure ranges from 12-22 mmHg and beyond that range is considered ocular hypertension. High pressure alone does not cause glaucoma, however, it is the only significant risk factor that is modifiable to date [3]. Evidence shows that IOP reduction slows the onset and progression of glaucomatous damage in eyes with primary open angle glaucoma [4]. The pressure builds up due to an imbalance between inflow and outflow of aqueous humour in the anterior chamber of the eye. One approach in managing glaucoma is to closely monitor the IOP and control it by either surgical or pharmaceutical strategies. Surgical methods that help to enhance fluid drainage involve a combination of invasive acute interventions such as canaloplasty, trabeculectomy, and endoscopic cyclophotocoagulation, or chronic implants such as micro shunts (stents) [5]. Pharmaceutical treatments, however, include non-invasive eye drops that either reduce the production of the aqueous humour, such as beta-blockers, or enhance fluid outflow, such as prostaglandin.

Among the many different technologies, Goldmann tonometry is the gold standard for IOP measurement. However, it is not a portable device, requires sterilization, and is operated by professionals in clinical settings. Although handheld devices such as the Tonopen® [6] are portable and can be used for more frequent measurements, they require temporary corneal anaesthesia, cost a few thousands of dollars, take a skilled operator to perform the measurement, or at the very least require high dexterity, and interrupt the regular flow of the user's life. This can significantly reduce the number of data points that can be obtained seamlessly in parallel with the user's daily activities at home or work. Previous studies demonstrate that IOP fluctuates continuously over time and may spike during night hours after (or before) patients see their physicians [7]. Therefore, continuous IOP measurement is necessary for providing individualized feedback that helps physicians monitor the disease progression and personalize their medical interventions tailored for the patient. These data also can be used by medical researchers in understanding the disease and finding novel correlates that could one day help to completely cure glaucoma and defeat its adverse effects.

Microelectromechanical system (MEMS) technologies have recently shown great promises in addressing certain ocular diseases, such as glaucoma, retinitis pigmentosa, and age-related macular degeneration [8]. In particular, MEMS-based IOP sensors provide numerous advantages compared to conventional tonometry techniques: continuous self-monitoring of IOP fluctuations throughout day and night and

1. *Electrical and Computer Engineering Department, Michigan State University, East Lansing, MI, USA.*
2. *Department of Mathematics, Michigan State University, East Lansing, MI, USA.*
3. *Department of Physiology, Michigan State University, East Lansing, MI, USA.*

ease of operation during the patient's ordinary routine. MEMS-based IOP sensors fall into two categories: implantable and wearable. One of the earliest implantable sensors, made in 1967, leveraged change in mutual inductance between two single-layer flat spiral coils spaced 0.05 mm apart and packed inside a 5-mm-diameter glass bubble [11]. Their tests on rabbits showed a response of 100 kHz/mmHg. Even though it had a small footprint and offered low cost by simple design, it suffered significantly from poor reading distance and its vulnerability to the variable orientation of the implant.

A common approach used in modern IOP sensors is based on implantable capacitive membranes, which are theoretically capable of measuring absolute IOP relative to a pre-set pressure of a sealed miniaturized chamber. These implants are either placed in the eye's anterior chamber [10-13] or accessed by aqueous humour through a needle inserted into the eye at the pars plana [14-15]. The capacitor membrane deflects due to pressure variance outside of the sensor chamber and causes a change in the electrical capacitance. The sensor can be configured into a passive RLC (resistor-inductor-capacitor) resonant circuit so that the capacitance variations are interrogated wirelessly by inductive coupling. An example using this design was reported by Chen et al. [11], and achieved a pressure sensing of 1-mmHg resolution with more than 2 cm of distance between the sensor and reader. Active IOP sensors also have been reported by several groups based on the variable capacitance principle [12&15]. For example, Chen et al. reported a highly sophisticated IOP sensor which consists of a solar cell, a thin film lithium battery, a MEMS capacitive sensor, and integrated application specific circuits (ASIC) all-together in a 1 mm3, biocompatible glass housing [12]. The device has a 0.5 mmHg pressure sensing resolution. The combination of energy harvesting and low-power operation allows the sensor to achieve zero-net-energy operation in low light.

Beside variable capacitors, IOP sensors based on other sensing and implantable mechanisms have been reported. For example, two models of variable-inductor based IOP sensors have been proposed and investigated by Chen et al. [16]. The same group demonstrated an opto-mechanical sensor [17] for IOP measurement, where a needle-based suture-less Bourdon tube deforms linearly with the pressure difference between the encapsulated tube and the eye chamber. This deformation can be visualized with the movement of the pointing tip at the free end of the Bourdon tube. An optical micro implant has also been investigated by Lee et al. [18], in which a nanodot array is placed inside an optical cavity on top of a circular thin layer of black silicon with a total diameter of 1 mm. Pressure-dependent optical readout is obtained using a Zeiss SL-30 slit lamp with a detection distance of 12 cm. One other optical approach was reported by Fernandes et al. [19], where a micro-fabricated silicon diffraction-grating-array was attached to the choroidal tissue in the back of the eye and IOP variation was detected by monitoring slight changes in the color of the gratings caused by the pressure-induced subtle strain in the choroid. Besides implantation in the anterior chamber of the eye, Chitnis et al. [20] used a less invasive, vitrectomy-based, approach for device placement. In their approach, the transponder consists of three parts, a 30-gauge needle that penetrates the sclera and creates direct access of the aqueous humour to a capacitive pressure sensor and a planar coil that stays outside the eye and serves as the antenna.

While enabling measurement of absolute IOP, the implantable sensors require surgical operations which limit the user diversity and population to a small group of patients who already have undergone surgeries due to other ocular conditions, such as cataracts. Implantation of IOP sensors alone does not justify the potential risk of adverse effects for identified glaucomatous patients. Poor biocompatibility of most conventional materials can cause postoperative inflammation and toxicity on one hand, and biofouling on the other hand, which quickly degrades the sensing performance over time. Another drawback that is a primary disadvantage of the capacitive-pressure-sensing implants derives from leakage of their sealed chamber, which results in a shift in baseline pressure, leading to uncontrollable inaccuracy.

Wearable, contact lens-based sensors, in contrast, are promising approaches for continuous, non-invasive IOP monitoring. Multiple sensors have been developed inside a contact lens employing various sensing mechanisms such as strain gauge using piezo-resistive materials, variable capacitive or inductive elements. One of the very earliest contact lens sensors, which was developed back in 1974, incorporated a wire in its periphery along with a semiconductor and foiled transducers that changed their resistance with elongation [21]. In 2011, Laukhin et al. presented a piezoresistive polymeric sensing film cantered inside a soft contact lens and wired to a portable device that collects, processes and sends out data via Bluetooth to a computer [22]. Later, Tseng et al. proposed the idea of a single-turn planar coil that sits inside a contact lens and changes its diameter with IOP variation [23]. These developments, however, require wires tethered to instruments for signal readout, limiting the comfortability and mobility of the devices. Therefore, wireless contact lens sensors (WCLS) are proposed to eliminate the tethering effect. For example, the WCLS reported by Chiou et al. [24] consists of a capacitive circular ring, a radio frequency identification (RFID) chip, and an antenna embedded in a 200-μm-thick HEMA-based contact lens. The distance between the two plates of the capacitive ring varies as the curvature of the cornea changes. A pressure sensitivity of 4.4 fF/mmHg was achieved with a reading distance of 1cm under 26.5 dBm incident RF power at 920 MHz. More recently, a Swiss WCLS, SENSIMED Triggerfish®, was approved by the Food and Drug Administration (FDA). The device incorporates an embedded microscale strain sensor that responds to spontaneous circumferential changes at the corneoscleral junction and a coil antenna that transmits the data to an external reader coil attached around the eye cavity [25]. The reader coil is wired to a pocket-sized signal processing and storage unit. While promising, when the efficacy of this device was compared with Tonopen® pressure readings from

twenty patients, the results showed a poor correlation between the data obtained by the two measurement units [26]. In addition, the above WCLS solutions involve an active circuit chip that adds complexity and cost to the overall system.

Our solution to the above limitations is a passive, wireless sensor where a closed-loop of stretchable wires acts as both a strain sensor to detect the corneal deformation and as an inductive antenna for wireless data readout. Our approach relies on near-field, passive electromagnetic coupling, eliminating the use of electronic chips in the contact lens. Using a variable inductor for strain sensing resolves the chamber leakage issue and unwanted baseline shift normally seen in variable capacitor-based sensors. The serpentine morphology amplifies the stretchability of the coil and therefore improves its sensitivity to the change of central corneal curvature as a result of the pressure variation. Previously, we presented an invasive version of the variable inductor with a commercial surface mounted capacitor soldered to the ends of the serpentine wire. The device was implanted under a flap of sclera right at the corneoscleral junction in a porcine eye and reported a pressure responsivity of 57 kHz per mmHg of change in IOP [27]. Building on our prior work, here, we present a new, non-invasive, wearable WCLS that integrates a stretchable coil and a microfabricated capacitor in a doughnut-shaped contact lens made of thin polymer, as depicted in Fig. 1. The sensor comprises thin film metal layers made of gold, titanium, and copper for conductive layers, and the dielectric layer between the capacitor plates uses Parylene C. The soft, doughnut-shaped contact lens made of polydimethylsiloxane (PDMS) enables the conformal placement of the sensor over the curved cornea while maintaining the normal vision of the user. While tailored for IOP measurement of glaucoma eyes, our proposed strain sensing method could be used in many other biomedical applications where detecting deformation and/or change in strain and/or morphology is desired. In this paper we present the wearable WCLS shown in Fig. 1. The development of the reader electronics integrated with the glasses and its communication with a smart phone is not in the scope of this paper and is shown to conceptually illustrate a proposed method of application for the CLS we build. Our IOP measurements presented here are conducted using desktop impedance analyzer and computer.

RESULTS

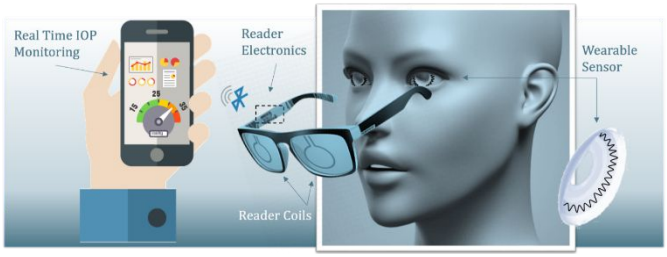

Figure 1: Concept diagram of the continuous IOP monitoring system. The wearable contact lens

Devices were microfabricated and integrated with custom-made contact lens as shown in Fig. 2. Fig. 2-a is a photomicrograph of the planar constant capacitor and junction point of the adjacent ends of the serpentine wire obtained using a polarizing microscope (Eclipse LV100, Nikon). Fig. 2-b is a photomicrograph of a capacitor being tested under the high voltage voltammogram. Fig. 2-c shows the sensor with a slight variation in the geometry encapsulated in the flexible doughnut-shaped contact lens made of PDMS next to a Roosevelt dime. Fig. 2-d shows a similar device with the original geometry. Fig. 2-e shows a doughnut-shaped contact lens being stretched and carried in a user's hand. Fig. 2-f shows the device being tested on the canine eye. A needle is inserted into the eye's anterior chamber which infuses saline for pressure control. The green reader coil measures the frequency response from the sensor's resonance circuit.

The stretchable inductor wire has an average length of 65.4 mm, a thickness of 500 nm, and a minimum width of 245 µm, resulting in an overall theoretical DC resistance of 13 Ω (Eq. V). The DC resistance of five devices are measured and averaged at 14.2 Ω which is in good agreement with the theoretical value. With a plate area of 700 × 880 µm2, the capacitance of the microfabricated capacitor is measured to be around 4.3 pF, which is close to the theoretical value of 4 pF (Eq. III). Notably, the 2-µm-thick Parylene dielectric is able to withstand voltages up to 1000 V without breaking down. The Inductance of the coil at rest is theoretically calculated at 27.4 nano Henrys (Eq. IV). which is in good agreement with the value obtained from COMSOL simulation: 26.7 nH. Fig. 2-f demonstrates that the contact lens sensor can be placed conformally on the cornea of the canine eye and coupled to an external reader coil (in green). The results from the bench-top characterizations of the sensor response to strain are reported in Table I and depicted in Fig. 3.

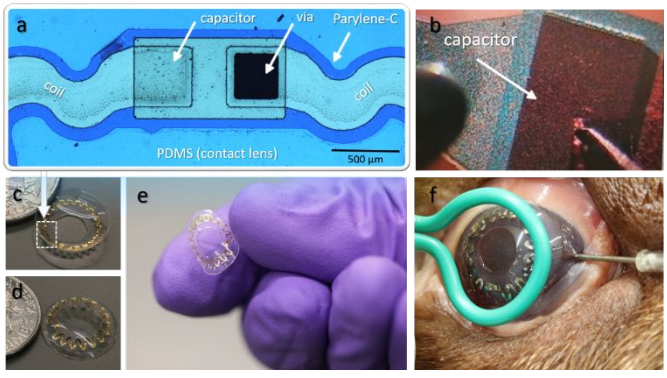

Figure 2: Fabricated devices. a) A microscopic image from the sensor's capacitor junction where the two ends of the coil meet and overlap. b) A microscopic view at the microfabricated capacitor while being tested under the high voltage cyclic voltammogram. c) The contact lens next to a Roosevelt dime (bottom-view) d) The contact lens next to a Roosevelt dime (top-view) e) The contact lens sensor held and flexed in a hand f) a look at the conformal placement of the contact lens sensor on the cornea of the canine eye.

Table 1: Results from bench-top measurements using the air chamber and the PDMS membrane setup.

State # (Experiment) ⇨	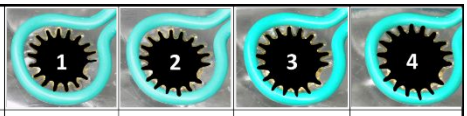			
Coil's Inner Area (mm^2)	55.4	60.25	68.56	76.82
Resonance Frequency (MHz)	494	486	480	476
Applied Pressure (mmHg)	4.5	13.5	19.5	25.5
Radius of Curvature (mm)	82.3	73.3	64.5	61.2
Simulated Inductance (nH)	26.7	27.7	29.2	30.6
State # (Simulation) ⇨	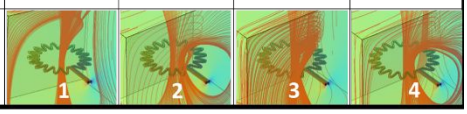			

During the measurements, a syringe infuses 5 ml of air into the chamber at each step and does that for three times, creating 4 different pressure points: 4.5 (no infusion), 13.5, 19.5, and 25.5 mmHg. The pressure increases in a nonlinear fashion since the PDMS membrane responds to the pressure in a nonlinear fashion. The radius curvature of the PDMS membrane at each step and the corresponded coil area are obtained using post-processing of the top-view images of Table I (first row) and complementary side-view images as illustrated in Fig. 3-a. The area of the coil loop increases proportionally with each step in pressure, illustrating the almost linear relationship between them, as presented in Fig. 3-b. A responsivity of 853 kHz per 1 mm change of the central radius of curvature is achieved on the PDMS membrane as shown in Fig. 3-c. Using a cantilever beam model [36] this responsivity can also be presented in the form of strain as follows:

$$\varepsilon = 100 \times \frac{R_2 - R_1}{R_2} \qquad \text{(I)}$$

where ε represents the axial strain in terms of percentage, R_1 denotes the radius of curvature of the PDMS membrane at rest (zero strain), and R_2 indicates the radius of curvature of the PDMS membrane at which the corneal strain is measured at. Using the four data points depicted in Table I, we observed 34.4% of strain across a range of 18 MHz frequency shift. This relationship is almost linear with an R-squared value of 0.9887. Using that linear relationship we calculate a final value of 523 KHz frequency shift per 1% of axial strain on the cornea.

Fig. 3-d shows the in vitro measurement of the sensor responses, where a total downshift of 2 MHz in frequency is detected with a 59 mmHg increase in pressure. This leads to a responsivity of 44 kHz/mmHg for the doughnut-shaped PDMS lens sensor. It is important to note the limitations of our current testing results. First, the eye of the isolated canine head (in vitro) used in our trial was frozen for weeks and thawed right before the experiment. That could affect the cellular matrices of the tissue, weaken the resistivity of the tissue to stress, and amplify the successive strain. Second, the ocular rigidity and subsequently the biomechanical responsivity of the corneal and scleral tissue to IOP fluctuations differs significantly from in vitro to in vivo tissues [37]. Third, a previous study [38] showed

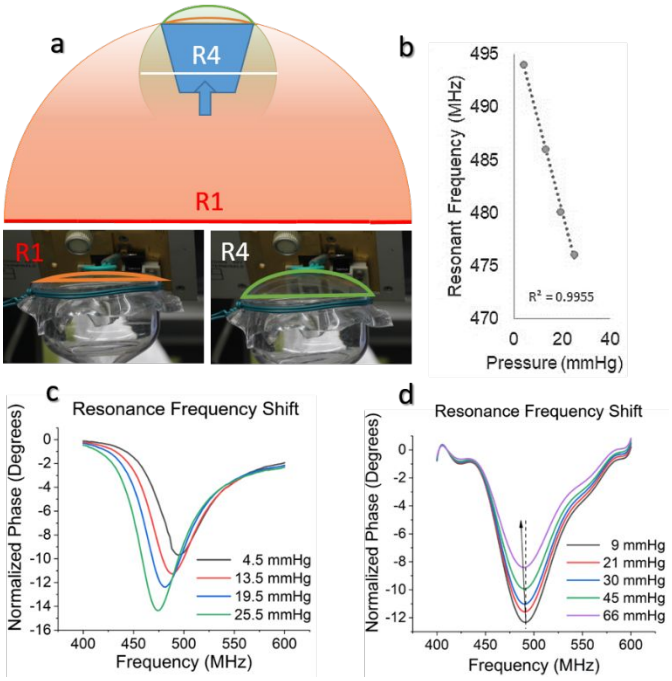

Figure 3: Bench-top and in vitro IOP measurements. a) The PDMS membrane testing apparatus: The radius of curvature (RC) changes from R1 to R4 when the rise in pressure deflects the membrane and lowers the RC. b) The linear relationship between the change in pressure and frequency response. c) The frequency response to the change of the central radius of curvature on the PDMS membrane. d) The resonance frequency shift caused by the induced change in the canine IOP in vitro.

that excised human eyes show a lower corneal hysteresis (therefore, higher responsivity to IOP) compared with intact living human eyes, which is important to consider when comparing results from enucleated eyes versus intact eyes. Fourth, in another study [39], human corneas were shown to be significantly stiffer than porcine corneas, which could perhaps be the case if the porcine corneas are not necessarily much different from the canine. Our current design is specifically tailored to canine eyes. Different device geometries and materials are under investigation to accommodate individual eyes across diverse animal models and eventually various human patients.

The effect of the planar angle between the reader and sensor coils on the sensing performance was tested under 4 different angles, and the results are shown in Fig. 4-a. The data show that the angular misalignment does not cause any shift in the resonant frequency of the sensor, and the signal is still detectable up to an extreme angle of 60°. Additional testing shows in Fig. 4-b that differences in distance between the reader and sensor coils does not change the frequency of the resonant peak. These results suggest that eye movements would not produce significant errors in pressure reading, but rather a reduction in the signal strength. The maximal reading distance of the current design is about 9 mm, which can be improved in the future by refining the sensor coil geometries (e.g. number of the loops, diameter, and thickness) and/or increasing power in the reader coil. The reproducibility of the sensor undergoing repeated inflations and deflations was tested under 10 cycles of iteration. Fig. 4-c shows that repeated

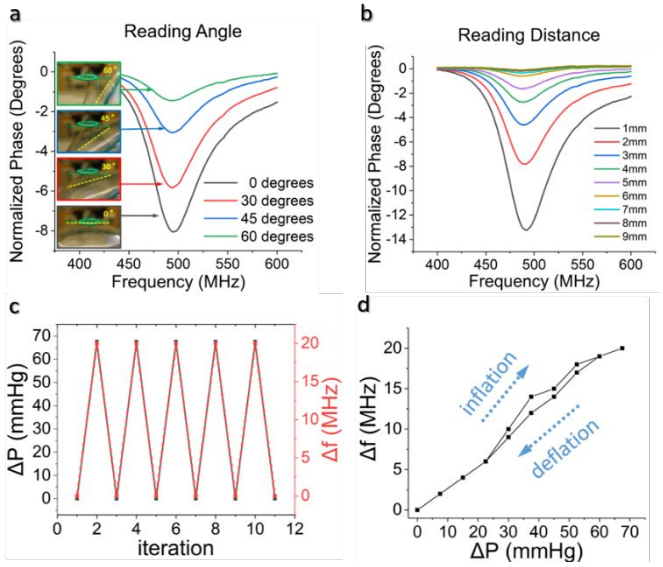

Figure 4: a) Frequency responses of the sensor under different planar angles between the reader and sensor coils. b) Frequency responses of the sensor under different distances between the reader and the sensor coils. c) Repeatability test results of the pressure response in five periods of inflation and deflation. d) Frequency shift in one cycle of inflation and deflation with finer pressure steps uncovering the negligible value of hysteresis.

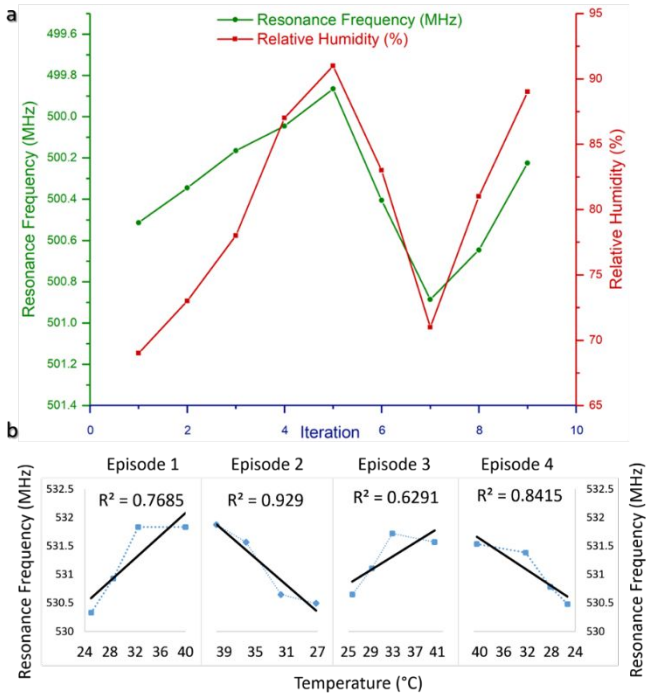

Figure 5: The change in the resonant frequency follows the trend of ARH change- repeated in three episodes. b) The change of the resonant frequency follows the trend of temperature change- repeated in four episodes.

stretching and relaxation of the sensor loop does not affect the baseline resonant frequency, demonstrating the stability of the sensor. Within one cycle, an overall frequency shift of 20 MHz is detected when ΔP changes from 0 to 68 mmHg. The deflation response exhibits a negligible hysteresis effect as compared to the inflation response, as shown in Fig. 4-d.

Finally, we studied the effects of environmental parameters (humidity and temperature) on the sensing performance of the device. The contact lens with the embedded sensor was placed inside a beaker next to a commercially available sensor (Temperature and Humidity Monitor- TP-50, ThermoPro) and the entire beaker was covered with plastic wrap. Using this apparatus the humidity is adjusted (when the beaker is uncovered) fast enough that the desired dynamic range for humidity is attainable without a significant change in temperature (<2°C). Therefore, we could isolate the effect of change in humidity on the contact lens from the effects of temperature fluctuations. In a separate apparatus, the contact lens with the embedded sensor was placed on top of a hot plate covered with aluminium foil and the temperature varied while being monitored by an infrared thermometer (Infrared Thermometer-IRT0421, Kintrex). In this setup, even though the temperature on the contact lens sensor varied over a high dynamic range, humidity remained essentially unchanged due to the free flow of the surrounding air.

Fig. 5-a depicts the resonant frequencies of the sensor under different ambient relative humidity (ARH) values of 69% to 91%. Within one and a half cycle of the ARH change, it is found that the resonant frequency of the sensor follows the trend of the ARH change. There is a downshift in the resonant frequency with an increase in ARH. This is caused by the swelling of the PDMS contact lens when ARH increases [20], resulting in an expansion of the coil curvature. When ARH reduces to its original value, the PDMS contact lens shrinks and the resonance frequency upshifts. The third half-cycle shows a similar trend. Additional experiments are conducted to analyse the effect of ambient temperature (AT), during which the sensor undergoes repeated heating and cooling and the device frequency response is measured in a temperature range of 25°C to 40°C that encompasses the AT change of the cornea. Fig. 5-b shows the four episodes of measurements that each presents half a cycle. When the AT increases from 25°C to 40°C, the PDMS contact lens shrinks [40], and therefore the resonant peak of the sensor upshifts to the higher frequency range. When the AT drops to 25°C, the resonant peak returns to its original frequency with a repeatable profile. These results suggest that the effects of AT and ARH on the sensor performance can be predicted, calibrated, and cancelled by the design of the future, measurement unit with built-in humidity and temperature sensors.

Discussion

This report presents a wireless, passive, sensor inside a doughnut-shaped contact lens that enables continuous monitoring of the change in the curvature of the cornea induced by IOP variation. This sensor consists of a stretchable coil and a micro-fabricated capacitor that is made of gold and titanium thin films sandwiched between multilayer Parylene C for extra biocompatibility. The sensor is completely encapsulated inside a doughnut-shaped contact lens made of PDMS which is soft, biocompatible, and permeable to moisture and gas. The strain sensor is tested separately in a PDMS membrane, showing a responsivity of 523 kHz of frequency shift per 1% axial strength.

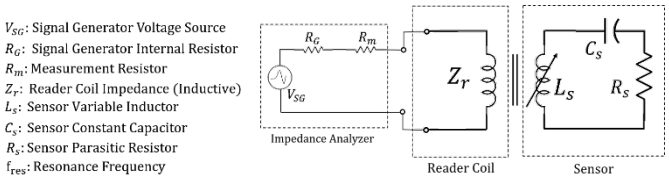

Figure 6: Circuit model for the continuous IOP monitoring system.

In vitro measurements on a canine eye demonstrate a responsivity of 44 kHz shift per 1 mmHg of pressure change. While consistent and measurable, the responsivity of the doughnut-shaped contact lens sensor is less on the canine eye compared with measurements of the device alone. This may be due to the quality of the corneas from the isolated eye, or imperfect conformity, and thus adhesion, of the lens to the test eye. Additional testing demonstrated that differences in the planar angle between the IOP sensor and external reading coil reduced the signal strength, but not the resonant frequency response of the sensor, thus indicating that eye movement does not produce significant errors. Repeated stretching and relaxation of the sensor ring also does not affect the baseline resonant frequency. Ambient relative humidity and temperature can cause shifts in resonant frequency, but these too track back to baseline when each factor returns to its starting point.

MATERIALS AND METHODS

Principles of operation and design

Our sensor is designed based on passive electromagnetic telemetry [28-32] which does not require an internal power source as seen in active sensors. The sensor device operates as an RLC resonator circuit (Fig. 6) including a capacitor (C), an inductor (L), and a resistor (R) in a passive fashion. Change in either one or two of these three elements can be detected by reading a shift in the resonance frequency of the resonant tank. When deformed under different IOPs, our device has a constant capacitance, a significant change in the inductance, and negligible change in the resistance, resulting in a shift in the resonance frequency as depicted in the equation below.

$$f_{res} = \frac{1}{2\pi}\sqrt{\frac{1}{L_s C_s} - \frac{R_S^2}{L_s^2}} \Rightarrow f_{res} \cong \frac{1}{2\pi}\sqrt{\frac{1}{L_s C_s}} \qquad (II)$$

The capacitor is modeled as a fixed, double plate capacitor, and the capacitance (C) can be estimated using the following equation for ideal double plate capacitors.

$$C = \varepsilon_0 \varepsilon_r \left(\frac{A}{t}\right) \qquad (III)$$

where ε_r is the relative permittivity of the dielectric material, ε_0 is the vacuum permittivity, A is the overlapping area between the capacitor plates, and t is the thickness of the dielectric material or the separation between the plates of the capacitor. Based on Perry's approximate formula [33] the theoretical strain-sensitive inductance (L) can be calculated using Equation III:

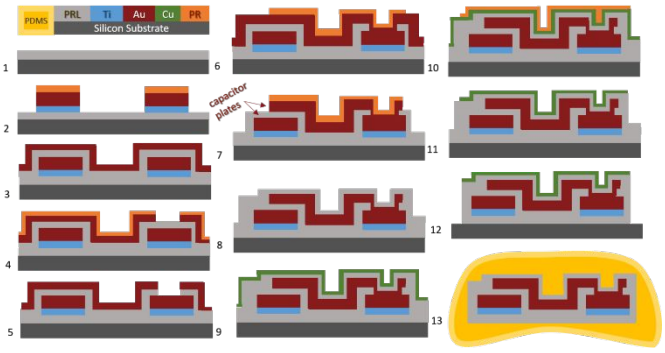

Figure 7: Fabrication step: 1) Deposition of Parylene C. 2) Patterning the deposited first metal layer. 3) Depositing the second Parylene-C layer. 4) Patterning the second metal layer. 5) Etching the Parylene-C away through the open via. 6) Depositing the third metal layer. 7) Wet etching the third metal layer. 8) Depositing the third Parylene-C layer. 9) Depositing the fourth masking metal layer. 10) Photolithography for patterning the masking metal. 11) Wet etching the fourth metal layer. 12) Dry etching Parylene-C. 13) Placing the released devices within the doughnut-shaped contact lens during the PDMS molding process.

$$L = \frac{4\pi n^2 a^2}{0.2317a + 0.44\,b + 0.39\,c} \qquad (IV)$$

where n is the number of turns of the coil, a is the mean radius of the coil, b is the width of the rectangular-cross-section wire that the coil is made of, c is the thickness of the same wire. When the serpentine wire stretches, the shrinkage or expansion of the coil varies the mean radius and causes a proportional change in the value of inductance, leading to an upshift or downshift of the resonant frequency.

The effect of the resistance can be neglected when the parasitic resistance is low. The following equation shows the overall resistance (R) across the serpentine wire:

$$R = \rho\frac{l}{A} \qquad (V)$$

where ρ is the electrical resistivity of the material, l is the length of the serpentine wire, A is the area of the cross section of the serpentine wire. Therefore, the material and the device geometry must be carefully designed such that the resistance of the wires is low enough to be negligible. In this case, the resonator is in the underdamped mode. The low resistance also enables high quality factor (Equation V) which sets the fundamental limit for the detectable range of the resonance peak.

$$Q = 2\pi f_{res}\frac{L}{R} \qquad (VI)$$

In order to obtain an accurate model of the coil and its expansion we mathematically modeled the circular serpentine wire with a polar equation as follows:

$$r(\theta) = p + q\left(\sin(n\theta)^4 - \frac{1}{2}\right) \qquad (VII)$$

p is the total radius of the serpentine circular coil, q is amplitude of the oscillation of the serpentine waves and n is the number of oscillations (n=18 in this case). The total circumference of the

curve (the length of the wire) is given by the polar arc length formula:

$$\text{Length} = \int_{\theta=0}^{2\pi} \sqrt{r^2 + \left(\frac{dr}{d\theta}\right)^2}\, d\theta \qquad \text{(VIII)}$$

Then, we calculate this integral numerically and find the enclosed area of the coil using the following polar area formula:

$$\text{Area} = \int_{\theta=0}^{2\pi} \frac{1}{2} r^2 d\theta \qquad \text{(IX)}$$

In our program executed inside Mathworks Matlab R2018b, we started with a given wire with fixed length and constant number of geometrical oscillations but flexible values for p and q. We numerically, then investigated how p and q change under various percentile changes in the enclosed area corresponding to our experimental values as shown in Table I. Eventually, the four chosen areas corresponding to the four experimental measured data points are imported as CSV files into AutoCAD 2016 as a curve, turned into complete 3D structures and then imported into COMSOL Multiphysics 5.4.0.346 for deriving their electrical inductance.

Sensor materials

A silicon substrate is used as a temporary carrier substrate for device microfabrication because it has reasonably good adherence with Parylene C. Parylene C serves as the structure and packaging material of the device because of its excellent biocompatibility (ISO 10993 & USP Class VI), mechanical flexibility (<200% elongation-to-break), optical transparency (<70% transmittance after 300nm), low moisture/gas permeability (water vapor transmission rate of 0.08 g·mm/m^2/day), and conformal coating using room-temperature chemical vapor deposition (CVD) [34]. Parylene C also is used as a dielectric layer of the microfabricated integrated capacitor due to its good dielectric strength (6,800 V/mil) [35]. The contact lens is made of polydimethylsiloxane (PDMS) which enables good stretchability and biocompatibility. For the main conductive material, gold is the material of choice because of its high biocompatibility and corrosion resistance. Copper is used as a sacrificial material to mask the packaging Parylene C in the plasma etching steps, and is completely removed from the final device to avoid toxic copper residuals in the ocular environment. A thin layer of titanium is used as an intermediate layer to improve the adhesion between the thin film layers of Parylene C and gold.

Sensor fabrication process

First, a 4-inch silicon wafer is coated with 4 µm Parylene C (PDS 2010 Labcoter® 2, Specialty Coating Systems) (Fig. 7-1). Then a layer of 20 nm titanium and 500 nm gold is thermally evaporated (Auto 306 Thermal Evaporator, Edward) on the wafer and patterned using ultra-violet (UV) photolithography to form the serpentine metal wire and the bottom plate of the capacitor (Fig. 7-2). After that, the wafer is coated with a 2 µm layer of Parylene C and a subsequent 20 nm of titanium and 150 nm gold (Fig. 7-3). This metal layer is patterned to form the top plate of the capacitor. A via is etched through metal using wet chemical etching (Fig. 7-4) and then through Parylene C using oxygen plasma with a photoresist mask (Fig. 7-5) to gain access to the first metal layer. The oxygen plasma etching is performed in a reactive ion etcher (RIE-1701, Nordson March) with a radio frequency (RF) power of 200 Watt and processing pressure of 150 mTorr. After that, the third metal layer of 350 nm gold is deposited onto the wafer which electrically connects the first and second metal layers through the Parylene via (Fig. 7-6). The top plate of the capacitor is formed by UV photolithography and chemical etching with a photoresist mask (Fig. 7-7). The third layer of 4-µm-thick Parylene C is deposited on the wafer for packaging the entire device (Fig. 7-8). Then a 200-nm-thick copper layer is thermally evaporated (Fig. 7-9) and patterned (Fig. 7-10) to mask and protect the desired areas during the subsequent Parylene C etching in RIE (Fig. 7-11). After the surrounding unwanted Parylene C is etched off, the copper mask is removed and devices are released from the silicon substrate using minimal nudge by a tweezer inside water (Fig. 7-12). Prior to testing, the devices are rinsed with acetone, isopropyl alcohol, and deionized (DI) water to remove photoresist and metallic residuals.

After the devices are released from the silicon substrate, a cast molding method is used to integrate the Parylene encapsulated sensor inside a doughnut-shaped PDMS contact lens (Fig. 7-13). Two plastic molds with concave and convex profiles that match the eye curvature are used. During the process, PDMS is prepared by mixing the curing agent and PDMS monomers (Sylgard 184, Dow Corning) in a ratio of 1:8. After the sensor is placed on the dome-shaped convex cap, the mixed PDMS is poured into the bottom concave mold. The top convex mold is aligned and pressed into the concave mold, and the thin gap between the molds defines the desired thickness of the PDMS contact lens, which is about 180 µm. The lens then is baked on a hotplate at 50°C for two hours until the PDMS is completely cured. After the central area of the lens is removed using a circular puncher, the doughnut-shaped contact lens is released from the mold carefully with the sensor encapsulated inside the PDMS, and ready for device testing.

Sensor characterization in a controlled pressure chamber

The capacitance and the breakdown voltage of the microfabricated Parylene-based capacitor are measured using a 4280A 1 MHz C Meter/C-V Plotter (Hewlett Packard) during a high voltage cyclic voltammetry up to 500 V generated using a Keithley high voltage source meter. The DC parasitic resistance is measured using a digital multimeter (VC890C, Victor). To evaluate the strain sensing performance of the device prior to the PDMS encapsulation, a bench-top setup was constructed which consists of a pressurized air chamber sealed by a top deformable PDMS membrane. The chamber is connected to a syringe from the bottom, which controls the volume of air through a syringe pump. During the infusion cycle of the pump, the pressure inside the chamber is raised and pushes the

membrane up, which causes the sensor to expand. As a result, the coil diameter increases, corresponding to an increase in the inductance value and a decrease in the resonant frequency of the RLC circuit. Computer simulations using COMSOL Multiphysics 5.4.0.346 are shown in the last row of Table I and they depict the consistent increase in the inductance values from the resting state towards expansion. During the refill cycle of the pump, the pressure inside the system goes down, and the membrane collapses and regains its radius of curvature. This reduces the radius of the coil, resulting in a decrease in the inductance and therefore an upshift of the sensor resonant frequency. The frequency response of the sensor is measured by coupling the sensor coil to an external coil antenna that is connected to an RF impedance analyzer (HP 4191A, Hewlett Packard), and the chamber pressure is simultaneously measured using a pressure gauge (Traceable Pressure Meter, Control Company)

Ex vivo characterization on canine eye

An ex vivo experiment was performed to validate the functionality of the doughnut-shaped PDMS contact lens sensor on a canine eye. In this case, a micro-syringe (gauge number: 23s) was used to inject saline into the anterior chamber of the eye in order to elevate the IOP, and refilled to remove saline from the eye and thus reduce the pressure. The actual IOP was measured using a pressure gauge that was connected to the micro-syringe. Similar to the bench-top setup, a single-loop reader coil was placed in close proximity to the sensor coil in order to detect the pressure-dependent frequency response of the sensor. The canine eye was retained in the orbit in the fully-isolated head with intact bones, tissues, and hair to better mimic the in vivo environment.

ACKNOWLEDGMENTS

The authors would like to acknowledge the financial support from the Michigan State University Foundation under the Targeted Support Grants for Technology Development (TSGTD).

CONFLICT OF INTEREST:

The authors declare that they have no conflict of interest.

CONTRIBUTIONS

M. H. M. Kouhani designed the stretchable serpentine strain sensor and together with Dr. Wen Li they micro-fabricated and tested devices and with help from Dr. Arthur J. Weber they created custom-made contact lenses and tested them on the canine eye. Jiajia Wu contributed in simulating the inductance of the stretchable coils in COMSOL Multiphysics and Arman Tavakkoli helped with mathematical modelling of the serpentine wires in Matlab.

REFERENCES

[1] Scott AW, Bressler NM, Ffolkes S, Wittenborn JS, Jorkasky J. Public attitudes about eye and vision health. JAMA ophthalmology. 2016 Oct 1;134(10):1111-8.

[2] Merepa SS, et al. Socioeconomic Influence of Glaucoma on Patients. EC Ophthalmology 9.1. 2018: 03-09

[3] Hommer A. Managing Primary Open-angle Glaucoma–Ocular Tolerability, Compliance, Persistence and Patient Outcomes. Eur Ophthalmic Rev. 2009;3:19-22.

[4] Kass MA, Heuer DK, Higginbotham EJ, Johnson CA, Keltner JL, Miller JP, Parrish RK, Wilson MR, Gordon MO. The Ocular Hypertension Treatment Study: a randomized trial determines that topical ocular hypotensive medication delays or prevents the onset of primary open-angle glaucoma. Archives of ophthalmology. 2002 Jun 1;120(6):701-13.

[5] Voskanyan L, García-Feijoó J, Belda JI, Fea A, Jünemann A, Baudouin C. Prospective, unmasked evaluation of the iStent® inject system for open-angle glaucoma: synergy trial. Advances in therapy. 2014 Feb 1;31(2):189-201.

[6] Nayak RR, Kandula P, Johri B, Pai SG, Kamath SJ. A Comparative Study of Intraocular Pressure Measurement Using Tonopen and Goldmann Applanation Tonometer. Hypertension. 2017;15:13-3.

[7] Chu E, Hamp A. IOP goes' bump'in the night: intraocular pressure rises during the night, hours after (or before) you see patients in your office. Here's a review of the latest research. Review of Optometry. 2011 Mar 15;148(3):73-9.

[8] Meng E, Yoon E, Gutierrez C. MEMS enabled technologies for ocular monitoring and therapy. InSolid-State Sensors, Actuators and Microsystems (TRANSDUCERS), 2017 19th International Conference on 2017 Jun 18 (pp. 379-382). IEEE.

[9] Collins CC. Miniature passive pressure transensor for implanting in the eye. IEEE Transactions on Biomedical Engineering. 1967 Apr(2):74-83.

[10] Koutsonas A, Walter P, Roessler G, Plange N. Implantation of a novel telemetric intraocular pressure sensor in patients with glaucoma (ARGOS study): 1-year results. Investigative ophthalmology & visual science. 2015 Feb 1;56(2):1063-9.

[11] Chen PJ, Saati S, Varma R, Humayun MS, Tai YC. Wireless intraocular pressure sensing using microfabricated minimally invasive flexible-coiled LC sensor implant. Journal of Microelectromechanical Systems. 2010 Aug;19(4):721-34.

[12] Chen G, Ghaed H, Haque RU, Wieckowski M, Kim Y, Kim G, Fick D, Kim D, Seok M, Wise K, Blaauw D. A cubic-millimeter energy-autonomous wireless intraocular pressure monitor. InSolid-State Circuits Conference Digest of Technical Papers (ISSCC), 2011 IEEE International 2011 Feb 20 (pp. 310-312). IEEE.

[13] Crum B, Li W. Parylene-based fold-and-bond wireless pressure sensor. InNano/Micro Engineered and Molecular Systems (NEMS), 2013 8th IEEE International Conference on 2013 Apr 7 (pp. 1155-1158). IEEE.

[14] Agarwal A, Shapero A, Rodger D, Humayun M, Tai YC, Emami A. A wireless, low-drift, implantable intraocular pressure sensor with parylene-on-oil encapsulation. InCustom Integrated Circuits Conference (CICC), 2018 IEEE 2018 Apr 8 (pp. 1-4). IEEE.

[15] Chitnis G, Maleki T, Samuels B, Cantor LB, Ziaie B. A minimally invasive implantable wireless pressure sensor for continuous IOP monitoring. IEEE Transactions on Biomedical Engineering. 2013 Jan;60(1):250-6.

[16] Chen PJ, Rodger DC, Saati S, Humayun MS, Tai YC. Microfabricated implantable parylene-based wireless passive intraocular pressure sensors. Journal of Microelectromechanical Systems. 2008 Dec;17(6):1342-51.

[17] Chen PJ, Rodger DC, Agrawal R, Saati S, Meng E, Varma R, Humayun MS, Tai YC. Implantable micromechanical parylene-based pressure sensors for unpowered intraocular pressure sensing. Journal of Micromechanics and Microengineering. 2007 Aug 31;17(10):1931.

[18] Lee JO, Park H, Chen O, Balakrishna A, Du J, Sretavan DW, Choo H. Achieving clinically viable 12-CM readout distance from micromachined implantable intraocular pressure sensor using a standard clinical slit lamp. InMicro Electro Mechanical Systems (MEMS), 2016 IEEE 29th International Conference on 2016 Jan 24 (pp. 210-213). IEEE.

[19] Fernandes J, Kwon YH, Kim JJ, Liu H, Jiang H. High Contrast Grating Based Strain Sensor for Intraocular Applications. Journal of Microelectromechanical Systems. 2018 Aug;27(4):599-601.

[20] Chitnis G, Maleki T, Samuels B, Cantor LB, Ziaie B. A minimally invasive implantable wireless pressure sensor for continuous IOP monitoring. IEEE Transactions on Biomedical Engineering. 2013 Jan;60(1):250-6.

[21] Greene ME, Gilman BG. Intraocular pressure measurement with instrumented contact lenses. Investigative ophthalmology & visual science. 1974 Apr 1;13(4):299-302.

[22] Laukhin V, Sánchez I, Moya A, Laukhina E, Martin R, Ussa F, Rovira C, Guimera A, Villa R, Aguiló J, Pastor JC. Non-invasive intraocular pressure monitoring with a contact lens engineered with a nanostructured polymeric sensing film. Sensors and Actuators A: Physical. 2011 Nov 1;170(1-2):36-43.

[23] Tseng CK, Huang YC, Tsai SW, Yeh GT, Chang CH, Chiou JC. Design and fabricate a contact lens sensor with a micro-inductor embedded for intraocular pressure monitoring. InSENSORS, 2012 IEEE 2012 Oct 28 (pp. 1-4). IEEE.

[24] Chiou JC, Hsu SH, Huang YC, Yeh GT, Liou WT, Kuei CK. A wirelessly powered smart contact lens with reconfigurable wide range and tunable sensitivity sensor readout circuitry. Sensors. 2017 Jan 7;17(1):108.

[25] Mansouri K, Goedkoop R, Weinreb RN. A Minimally Invasive Device for the Monitoring of 24-hour Intraocular Pressure Patterns. US Ophthalmic Review. 2013 Mar 1;6(1).

[26] Vitish-Sharma P, Acheson AG, Stead R, Sharp J, Abbas A, Hovan M, Maxwell-Armstrong C, Guo B, King AJ. Can the SENSIMED Triggerfish® lens data be used as an accurate measure of intraocular pressure?. Acta ophthalmologica. 2018 Mar;96(2):e242-6.

[27] Kouhani MH, Weber A, Li W. Wireless intraocular pressure sensor using stretchable variable inductor. InMicro Electro Mechanical Systems (MEMS), 2017 IEEE 30th International Conference on 2017 Jan 22 (pp. 557-560). IEEE.

[28] Núñez CG, Manjakkal L, Dahiya R. Energy autonomous electronic skin. npj Flexible Electronics. 2019 Jan 4;3(1):1.

[29] Chen PY, Sakhdari M, Hajizadegan M, Cui Q, Cheng MM, El-Ganainy R, Alù A. Generalized parity–time symmetry condition for enhanced sensor telemetry. Nature Electronics. 2018 May;1(5):297.

[30] Kim J, Kim M, Lee MS, Kim K, Ji S, Kim YT, Park J, Na K, Bae KH, Kim HK, Bien F. Wearable smart sensor systems integrated on soft contact lenses for wireless ocular diagnostics. Nature communications. 2017 Apr 27;8:14997.

[31] Chen LY, Tee BC, Chortos AL, Schwartz G, Tse V, Lipomi DJ, Wong HS, McConnell MV, Bao Z. Continuous wireless pressure monitoring and mapping with ultra-small passive sensors for health monitoring and critical care. Nature communications. 2014 Oct 6;5:5028.

[32] Cao H, Weber RJ, Hamouche NG. A passive intraocular pressure sensor and a wireless sensing technique using an intermediate LC resonator. InLife Science Systems and Applications Workshop (LiSSA), 2011 IEEE/NIH 2011 Apr 7 (pp. 5-8). IEEE.

[33] Rosa EB, Grover FW. Formulas and tables for the calculation of mutual and self inductance.(Revised.). Journal of the Washington Academy of Sciences. 1911 Jul 19;1(1/2):14-6.

[34] Scscoatings.com, 'SCS Parylene Properties.' Available: http://goo.gl/NNihZx [Accessed: 23-Jan-2019].

[35] Parylene.com, 'Para Tech Parylene Properties.' Available: https://goo.gl/qb7gvR [Accessed: 23-Jan- 2019].

[36] https://www.doitpoms.ac.uk/tlplib/beam_bending/bend_moments.php [Accessed: 15-Mar-2019].

[37] Pallikaris IG, Dastiridou AI, Tsilimbaris MK, Karyotakis NG, Ginis HS. Ocular rigidity. Expert Review of Ophthalmology. 2010 Jun 1;5(3):343-51.

[38] Alhamad TA, Meek KM. Comparison of factors that influence the measurement of corneal hysteresis in vivo and in vitro. Acta ophthalmologica. 2011 Aug;89(5):e443-50.

[39] Elsheikh A, Alhasso D, Rama P. Biomechanical properties of human and porcine corneas. Experimental eye research. 2008 May 1;86(5):783-90.

[40] onov L. Biomimetic hydrogel-based actuating systems. Advanced Functional Materials. 2013 Sep 25;23(36):4555-70.

Contact

*M. H. M. Kouhani, tel: +1-517-7759527; mhmk@msu.edu

.